Geophys. J. R. astr. Soc. (1975) 43, 425–451

A Physical Model for the Creation of the Lithosphere

Douglas W. Oldenburg*

(Received 1975 March 3)†

Summary

The physical model for the creation of the lithospheric plates described by Parker & Oldenburg is considered in detail and the method by which a solution was obtained is given in full. The effects of reducing the percentage of partial melt, adding radioactive material and allowing temperature gradients in the asthenosphere are considered. The model is sufficiently flexible to allow for the creation of a variety of lithospheric plates which predict elevations (except near the ridge crest), heat flow, and gravity in acceptable agreement with observations. The important prediction by the physical model that the lithosphere continually thickens with the square root of distance from the ridge has been verified in the laboratory by using the wax model of Oldenburg & Brune.

Introduction

The purpose of this paper is to present in detail the physical model for the generation of lithospheric plates described by Parker & Oldenburg (1973). The method for obtaining a complete solution will be developed in full, as well as the effect on the model of varying such parameters as the amount of partial melt, radioactivity, and some of the physical constants. It will be shown that this model, which is independent of convective processes existing beneath the lithosphere, predicts ridge elevation, heat flow and free air gravity anomalies in good agreement with empirical observations. In addition, the physical model can be realized in a laboratory experiment and the important prediction of a continual thickening of the lithosphere with distance from the ridge crest will be tested.

The physical model is basically a refinement of McKenzie's model for crustal creation (McKenzie 1967) to include the latent heat of fusion in the heat budget determining the growth of the lithosphere. The existence of an intrusion zone below the ridge crest and a continual thickening of the lithosphere as a function of crustal age are important consequences of this heat budget which have no counterpart in McKenzie's model.

Physical model

A two-dimensional system is considered, namely a vertical cross-section of the ridge system normal to its strike. The lithosphere is modelled by a solid slab overlying

* Present address: Institute for Earth and Planetary Physics, University of Alberta, Edmonton, Alberta T6G 2J1, Canada.

† Received in original form 1974 August 1

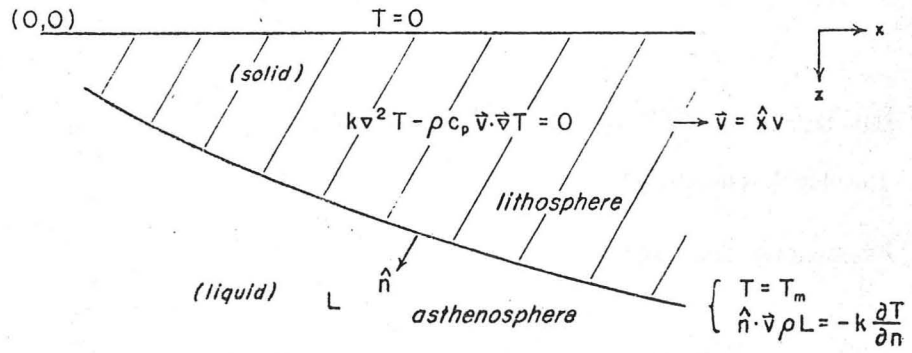

k	thermal conductivity
ρ	density
c_p	specific heat
v	plate velocity
$\hat{n}$	outward pointing normal
L	latent heat of fusion of the liquid

FIG. 1. Geometry of the lithosphere–asthenosphere system.

an isothermal fluid asthenosphere whose temperature is equal to the melting temperature, and the interface between these two regions is assumed to be the solid–liquid phase boundary of the material. If the melting temperature is assumed to be independent of depth then this boundary delineates the melting point isotherm. In a frame of reference fixed with respect to the ridge axis, we suppose that the lithosphere–asthenosphere boundary is invariant in time, even though the solid is moving horizontally. This can occur only if material is accreting onto the slab at exactly the right rate. Such growth, because it is a condensation of a liquid into a solid, releases latent heat that must be carried away by conduction to the surface. The boundary conditions on the solid–liquid interface, whose shape is to be defined, are therefore

$$\hat{n}.\vec{v}\rho L = -k\frac{\partial T}{\partial n} \tag{1}$$

$$T = T_m \tag{2}$$

where T_m is the melting temperature and the remaining parameters are explained in Fig. 1. Within the solid slab the temperature must satisfy the Eulerian steady state heat flow equation

$$k\nabla^2 T - \rho c_p \vec{v}.\vec{\nabla}T = 0 \tag{3}$$

with

$$T(x, 0) = 0\,^\circ\text{C}. \tag{4}$$

The right-hand side of equation (3) has been set to zero since we shall assume that no heat sources exist in the slab, and the oceans constitute such a large thermal reservoir that (4) is true to a very good approximation. Equations (1)–(4) are not self-consistent and lead to a physical paradox. To see this we can examine the region sufficiently close to the origin such that the temperature satisfies Laplace's equation. If the melting temperature boundary meets the surface at the origin, not only is the vertical heat flux infinite at that point, but the energy transported through any finite area containing the origin is infinite; yet equation (1) shows that the heat flow and hence the energy

flux must be bounded. This inco
conditions break down in the
conditions must be sought to a
upper surface.

Parker & Oldenburg resolve
model: they assume that materia
ridge crest and that this region is
$\bar{T}(z)$, is time-averaged over peri
is equated with the steady-state t
must always be greater than o
magma cools before the next ep
$\bar{T}$ and T_f is not known, but near
thought of as instantaneously re
the crack only a small error is in
equal to T_m. We shall set $\bar{T}$ =
heat budget equation along this

$$-k\frac{\partial T}{\partial x}$$

At the origin, equation (5) red
might have been inferred from e
often encountered in elliptic pr
ditions and presents no difficul
interpretation of such a problem

It is convenient to transform
all temperatures by T_m and all
resulting equations and boundar

$$\frac{\partial T}{\partial x}(0, z) = -$$

$$T(x, z) = 1$$

$$\frac{\partial T}{\partial n} = -\hat{n}.\hat{x}$$

where

is a dimensionless velocity and

* This equation is identical to equ
term $k|\nabla T|$ has been replaced by $-k$
and can be obtained either by integra
deriving it directly from pill-box argu

flux must be bounded. This inconsistency forces us to the conclusion that the boundary conditions break down in the vicinity of the ridge crest and that a different set of conditions must be sought to avoid the close approach of the T_m isotherm and the upper surface.

Parker & Oldenburg resolve the inconsistency by considering a simple geological model: they assume that material is intruded into a narrow, vertical crack beneath the ridge crest and that this region is modelled by a vertical line on which the temperature, $\bar{T}(z)$, is time-averaged over periods of active injection and subsequent cooling. $\bar{T}(z)$ is equated with the steady-state temperature used in equation (3), and this temperature must always be greater than or equal to $T_f(z)$, the final temperature to which the magma cools before the next episode of intrusion. The precise relationship between $\bar{T}$ and T_f is not known, but near the surface the magma cools so quickly that it may be thought of as instantaneously reaching T_f, hence $\bar{T} = T_f$ there. Near the bottom of the crack only a small error is incurred if $\bar{T}$ is set equal to T_f because both are nearly equal to T_m. We shall set $\bar{T} = T_f$ everywhere within the crack, and therefore the heat budget equation along this intrusion zone becomes

$$-k\frac{\partial T}{\partial x} = \rho v\left[L + c_p\left(T_m - T_f(z)\right)\right].* \tag{5}$$

At the origin, equation (5) reduces to $k\partial_x T = -\rho v(L + c_p T_m)$ and is not zero as might have been inferred from equation (4). However, such a point discontinuity is often encountered in elliptic problems with Dirichlet or Neumann boundary conditions and presents no difficulty either to the numerical solution or the physical interpretation of such a problem.

It is convenient to transform equations (1)–(5) into dimensionless form by scaling all temperatures by T_m and all distances by l, the length of the intrusion zone. The resulting equations and boundary conditions are

$$\nabla^2 T - 2u\frac{\partial T}{\partial x} = 0 \tag{6a}$$

$$T(x, 0) = 0 \tag{6b}$$

$$\frac{\partial T}{\partial x}(0, z) = -2u\left(H + 1 - T(z)\right) \qquad z \leqslant 1, \qquad x = 0 \tag{6c}$$

$$T(x, z) = 1{\cdot}0 \text{ on bottom of the lithosphere} \tag{6d}$$

$$\frac{\partial T}{\partial n} = -\hat{n}.\hat{x}2uH \text{ on bottom of the lithosphere} \tag{6e}$$

where

$$u = \frac{\rho c_p v l}{2k} \tag{7}$$

is a dimensionless velocity and

$$H = L/c_p T_m. \tag{8}$$

* This equation is identical to equation (3) in the paper by Parker & Oldenburg except that the term $k|\nabla T|$ has been replaced by $-k\partial T/\partial x$. The boundary condition given here is the correct one and can be obtained either by integrating the differential equation across the source region or by deriving it directly from pill-box arguments.

For every value of H a complete solution to these equations can be found to determine the dimensionless velocity u, the shape of the underside of the lithosphere, the length, l, of the intrusion zone, and the temperature everywhere within the slab.

The technique used to solve these equations is analogous to the method of images often used in potential problems. The lithosphere is embedded in an infinitely thick slab ($x \geqslant 0$, $z \geqslant 0$) which is moving horizontally with velocity v and shares all the physical properties of the lithosphere. Temperatures within this quarter space can be calculated from a knowledge of the temperature on the vertical axis and the Green's function appropriate to equations (6a) and (6b). The temperature distribution on the vertical axis is adjusted until a value of u is found to satisfy equation (6c) and simultaneously, equations (6d) and (6e) are obeyed on a curved line which meets the vertical wall at the base of the intrusion zone. The region above the curved line is clearly the lithospheric slab and the temperatures below are not physically significant.

The Green's function for this problem is derived in Appendix A and the relationship between the temperature on the vertical boundary and that at a point (x, z) is given by

$$T(x,z) = \int_0^\infty T(0,z')G(x,z;z')dz'$$

$$= \frac{ux\exp(ux)}{\pi}\int_0^\infty T(0,z')\left\{\frac{K_1'(ur_-)}{r_-} - \frac{K_1'(ur_+)}{r_+}\right\}dz' \qquad (9)$$

where K_1' is a modified Bessel function of order 1 and $r_+^2 = x^2+(z+z')^2$ and $r_-^2 = x^2+(z-z')^2$. As $x \to 0$, $G(x,z;z')$ acts as a delta function making equation (9) difficult to evaluate quickly and accurately, and therefore an alternate method of calculating the temperatures close to the vertical boundary is desirable. For this purpose, we consider a horizontal slab of finite thickness D with a surface temperature $T = 0$ and a bottom temperature $T(x, D) = T(0, D) = T_D$. The temperature within the region $x \geqslant 0$, $z \leqslant D$ is given by (McKenzie 1967)

$$T(x,z) = \frac{T_D z}{D} + \sum_{n=1}^{\infty} a_n \sin\left(\frac{n\pi z}{D}\right)\exp(-\gamma_n x) \qquad (10a)$$

$$\gamma_n = \sqrt{\left[\left(\frac{n\pi}{D}\right)^2 + u^2\right]} - u \qquad (10b)$$

$$a_n = \frac{2}{D}\int_0^D T(0,z)\sin\left(\frac{n\pi z}{D}\right)dz. \qquad (10c)$$

The coefficients a_n are the sine transform of $T(0, z)$ and are easily calculated by extending $T(0, z)$ as an odd function, discretizing, and computing the digital Fourier transform of the resultant series. The accuracy of the a_n's computed in this way degenerates with increasing n because of the assumed periodicity in the Fourier transform algorithm, but this error amounts to only a few per cent when $n \sim N/5$ (N is the total number of points in the series) and thus no difficulty is encountered even when the upper limit of the sum in equation (10a) is large. In general, for $x < 1{\cdot}0$ the temperatures were computed by the above method, while for $x \geqslant 1{\cdot}0$, the temperatures were computed by using equation (9).

To find a value of u and a temperature distribution on the intrusion zone such that equation (6c) is obeyed, we proceed as follows. A slab of thickness D ($D = 3{\cdot}0$ or $4{\cdot}0$ were found to be adequate) is used with an assumed initial temperature on the

vertical axis and value of u. An iterative technique is used to adjust the temperature for $z \leqslant 1$ while temperatures at greater depths remain fixed. For $0 \leqslant z \leqslant 1$ the horizontal temperature derivatives may be computed from equation (6c), while for $1 \leqslant z \leqslant D$ they may be determined from equation (10). The heat flow equation, with the specification of the normal derivative of temperature on the vertical wall, as well as temperatures on the upper and lower surfaces of the slab, has a solution given by equation (10a) with coefficients

$$a_n = -\frac{2}{\gamma_n D}\int_0^D \frac{\partial T}{\partial x}(0, z)\sin\left(\frac{n\pi z}{D}\right)dz. \tag{11}$$

The solution of this boundary value problem will not, in general, satisfy the condition that $T(0, 1) = 1{\cdot}0$, and the value of u must be adjusted such that this requirement is fulfilled. The updated value of u and the new temperature distribution are then used to calculate new values of the horizontal derivatives and the procedure is repeated. Convergence has been found to be rapid with acceptable accuracy attained after three or four iterations.

The shape of the underside of the lithosphere is determined by finding a curved line which extends outward from the base of the intrusion zone and on which equations (6d) and (6e) are simultaneously obeyed. The location of the melting point isotherm, $T = 1$, is easily calculated and the line on which equation (6e) is obeyed, the isofuse line, can be determined from the solution of a first order differential equation (see Appendix B)

$$\frac{dZ(x)}{dx} = \frac{\partial T/\partial z}{2uH + (\partial T/\partial x)} \qquad Z(0) = 1{\cdot}0. \tag{12}$$

For an arbitrary temperature distribution the isotherm and isofuse lines will not coincide and therefore adjustment to the boundary temperature below the intrusion zone is necessary. This adjustment is readily effected because of the constraints imposed by the existence of an asymptotic solution to equations (6). We shall first derive this asymptotic solution and later return to the question of how the adjustments are carried out.

At sufficiently large distances from the ridge crest, $ux \gg 1$, $\partial_x{}^2 T$ is negligible compared to $2u\partial_x T$ and the differential equation (6a) reduces to

$$\frac{\partial^2 T}{\partial z^2} - 2u\frac{\partial T}{\partial x} = 0. \tag{13}$$

If $T(x, 0) = 0$ and $T(0, z) = T_w = \text{constant}$, this system has a very simple solution (Carslaw & Jaegar 1959, p. 58)

$$T(x, z) = T_w\, erf\left(z\sqrt{\frac{u}{2x}}\right). \tag{14}$$

When equation (14) is substituted into equation (12) and evaluated on the boundary, $Z(x)$, we obtain

$$\frac{dZ(x)}{dx} = \frac{T_w\, erf'\left(Z(x)\sqrt{\frac{u}{2x}}\right)\sqrt{\frac{u}{2x}}}{2uH - \frac{T_w}{2x}\, erf'\left(Z(x)\sqrt{\frac{u}{2x}}\right)Z(x)\sqrt{\frac{u}{2x}}}. \tag{15}$$

The substitution

$$Z(x) = \alpha \sqrt{\frac{2x}{u}} \tag{16}$$

reduces this to

$$2H\alpha = T_w \, erf'(a) \quad \text{if} \quad 2ux \gg \alpha^2.$$

For any value of T_w, an α can be found which satisfies this relation and the location of the isofuse line is then directly obtained from equation (16). The demand that this line coincides with the melting temperature isotherm requires that $T_w = 1/erf(a)$, and hence, both conditions are satisfied if α is the solution to

$$2H\alpha \, erf(\alpha) = erf'(a). \tag{17}$$

It will be shown later that the range of values of H relevant to lithospheric problems require that u and α are in the order of 1, and thus the asymptotic approximation (16) is valid at distances greater than a few intrusion zone lengths away from the ridge crest.

The temperature structure on the vertical wall is therefore well constrained: for $0 \leqslant z \leqslant 1$ this temperature is chosen to satisfy equation (6c) and for depths greater than a few intrusion zone lengths the temperature must be very close to its asymptotic value T_w. There remains only a small segment of the vertical boundary along which the temperature must be adjusted to make the isotherm and isofuse lines agree, and this task is easily accomplished. This procedure will affect the value of u and the temperature distribution on the intrusion zone found from equation (6c) and these quantities should be recomputed if major adjustments have been made.

Numerical example

A numerical example will now be discussed and the predictions from the model compared with geophysical observations. We prescribe the following material parameters:

$$T_m = 1200\,^\circ\text{C}$$
$$c_p = 1{\cdot}05 \times 10^3 \text{ J kg}^{-1}\,^\circ\text{C}^{-1} \ (0{\cdot}25 \text{ calorie g}^{-1}\,^\circ\text{C}^{-1})$$
$$L = 4{\cdot}2 \times 10^5 \text{ J kg}^{-1} \ (100 \text{ calorie g}^{-1})$$
$$\rho = 3{\cdot}3 \times 10^3 \text{ kg m}^{-3} \ (3{\cdot}3 \text{ g cm}^{-3})$$
$$k = 2{\cdot}9 \text{ W m}^{-1}\,^\circ\text{C}^{-1} \ (7 \times 10^{-3} \text{ calorie cm}^{-1}\,\text{s}^{-1}\,^\circ\text{C}^{-1}).$$

The latent heat and melting temperature are typical of materials such as pyroxene or peridotite, and the other constants have been commonly used in thermal studies of ridges (Sclater & Francheteau 1970; McKenzie 1967). From these numbers $H = 0{\cdot}33$. The solutions to equations (6) yields a dimensionless velocity $u = 0{\cdot}60$ and a temperature along the intrusion zone which is shown in Fig. 14. Equation (7) indicates that the thickness of the intrusion zone varies inversely with spreading rate and that the constant of proportionality is determined by the numerical value of u. For this example, $vl = 32 \text{ m}^2 \text{ y}^{-1}$, so a ridge spreading with velocity 10 mm/year has an intrusion zone depth of 3·2 km. Petrological studies of marine basalts (Bass 1971) indicate that their depth of origin is indeed inversely related to spreading velocity, although the depth estimates of 20–50 km are much larger than our values. The thinness of the lithosphere at the ridge crest is supported by recent inversions of surface waves crossing the Pacific. Leeds (1974), using Rayleigh wave dispersion data, has indicated that this thickness is only a few kilometres and Forsythe (1974), inverting both Love and Rayleigh wave data, concluded that the average thickness in the region 0–5 My must be less than 30 km.

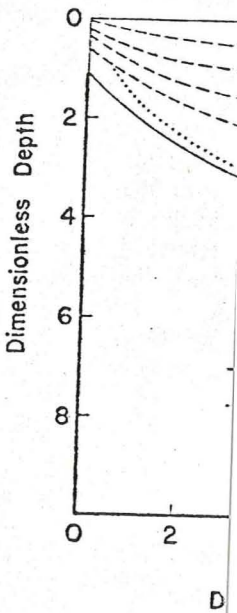

FIG. 2. Shape o
Dimensional q

The exact shape o
solution, is shown in
means that even for a
approximation at dis
asymptotic relation be

where t is given in mill
of (18) as a relationsh
sphere obtained by Le
at the ridge crest, 57 k
these thicknesses are i
non-uniqueness involv
indicates that the Rayl
ing lithosphere. Davis
tions as a function of t
between these quantiti
relationship is expecte
validity of equation (18
resorbed in the mantle
from the trench to the
the trench. The 11 di
linear relationship bet
resorption time of a su

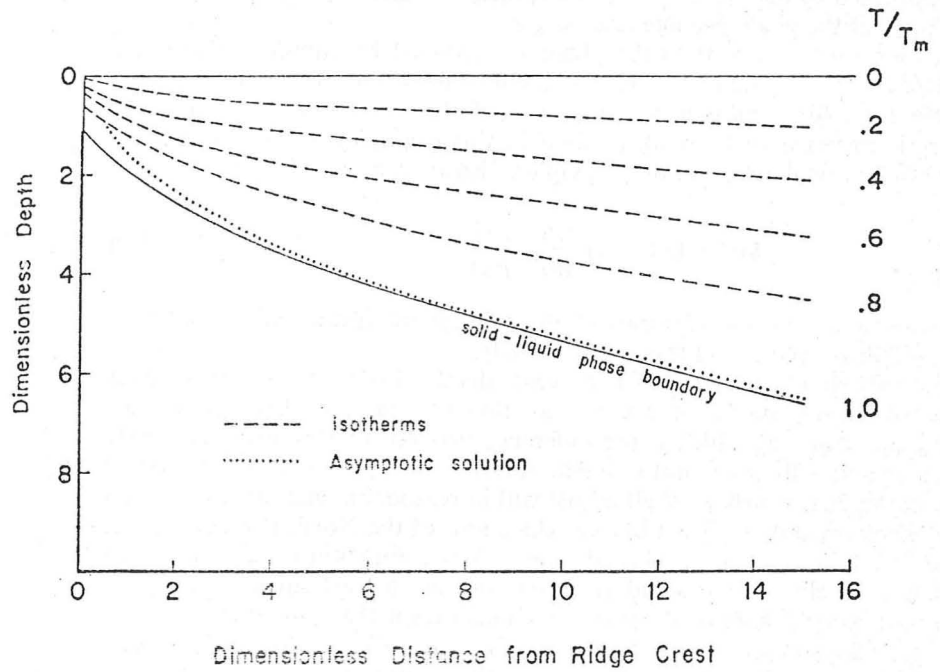

FIG. 2. Shape of the underside of the lithosphere and the asymptotic solution. Dimensional quantities can be obtained from the relationship $vl = 32\ \mathrm{m^2\ y^{-1}}$.

The exact shape of the underside of the lithosphere, as well as the asymptotic solution, is shown in Fig. 2. The close agreement between the two curves for $x > 3$ means that even for a spreading rate of 10 mm/year the asymptotic solution is a good approximation at distances greater than 10 or 15 km from the ridge crest. The asymptotic relation between crustal age and dimensional lithospheric thickness is

$$Z(t) = 35{\cdot}4\alpha\sqrt{\left(\frac{kt}{\rho c_p}\right)}\ \mathrm{km}$$
$$= 9{\cdot}5\sqrt{(t)}\ \mathrm{km} \qquad (18)$$

where t is given in millions of years. There is evidence supporting the functional form of (18) as a relationship between crustal age and lithospheric thickness. The lithosphere obtained by Leeds' inversion of Rayleigh waves has a thickness of about 8 km at the ridge crest, 57 km at 30 My, 90 km at 100 My and 157 km after 150 My, and these thicknesses are in good agreement with equation (18). There is a problem of non-uniqueness involved with such inversions, but at worst this qualitative agreement indicates that the Rayleigh wave data are not inconsistent with a continually thickening lithosphere. Davis & Lister (1974) have plotted empirical sea floor depth observations as a function of the square root of crustal age and obtained a linear relationship between these quantities for all ridges examined. We shall show that such a linear relationship is expected if the lithosphere thickens as $\sqrt{t}$. Additional evidence for the validity of equation (18) is that older oceanic plates require longer times to be thermally resorbed in the mantle (Deffeyes 1972). The resorption time is defined as the distance from the trench to the deepest earthquake, divided by the plate to plate closure rate at the trench. The 11 different plates, distributed in age from 9 to 130 My, suggest a linear relationship between the resorption time and the age of the sea floor. If the resorption time of a subducting plate is primarily determined by a diffusive process,

and hence is governed by the square root of time, then this linear relationship suggests that the thickness of the plate also increases as $\sqrt{t}$.

The increasing thickness of the lithosphere as predicted by equation (18) has a dominant effect on the elevation of the ridge crest, heat flow, and the observed gravity anomaly. We shall first consider the elevation of the ridge crest. Because the asthenosphere is assumed to be weak (a fluid in this example), the elevation at a crustal age t can be calculated from the principle of isostasy, and is given by

$$h(t) = (Z(t) - l)\frac{(\bar{\rho}_L - \rho_A)}{(\rho_A - \rho_W)} \tag{19}$$

where $\bar{\rho}_L$, ρ_A, and ρ_W are the densities of the lithosphere (mean value, vertically averaged), the asthenosphere and water, respectively.

Two comments should be made: The absolute depth of the crest below sea level is not predicted by this model, and the evaluation of equation (19) requires the knowledge of $\Delta\rho = \bar{\rho}_L - \rho_A$ which is the difference between two numbers of nearly equal magnitude and is therefore not well determined. Thus, we are forced to regard $\Delta\rho$ as a free parameter, which we shall adjust within reasonable bounds, to obtain a good fit to the empirical data. The observed elevations of the North Pacific (Sclater, Anderson & Bell 1971) have been plotted in Fig. 3 as a function of $\sqrt{t}$. The data were weighted inversely as their standard deviations and a least squares procedure was used to fit a straight line to all the observations except the value of $t = 0$. The rms deviation of the straight line from the data is 76 m and the slope of this line yields $\Delta\rho = 86\ \mathrm{kg\ m^{-3}}$. The calculated elevation, shown in Fig. 3, has been lowered by a constant value of 2783 m. This results in excellent agreement between the model

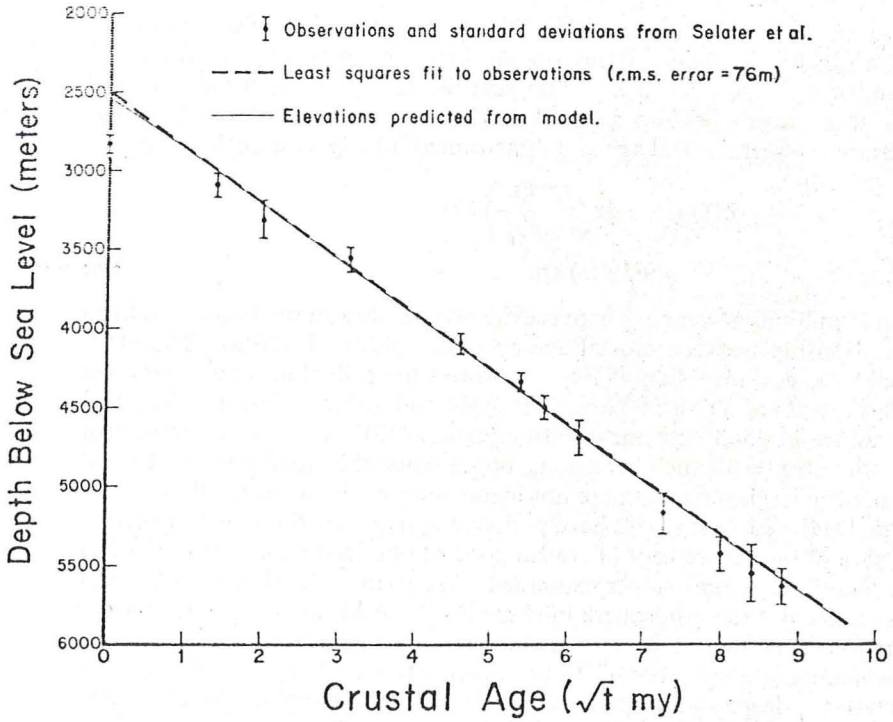

FIG. 3. Observed and predicted elevations for the North Pacific (observations from Sclater *et al.* 1971).

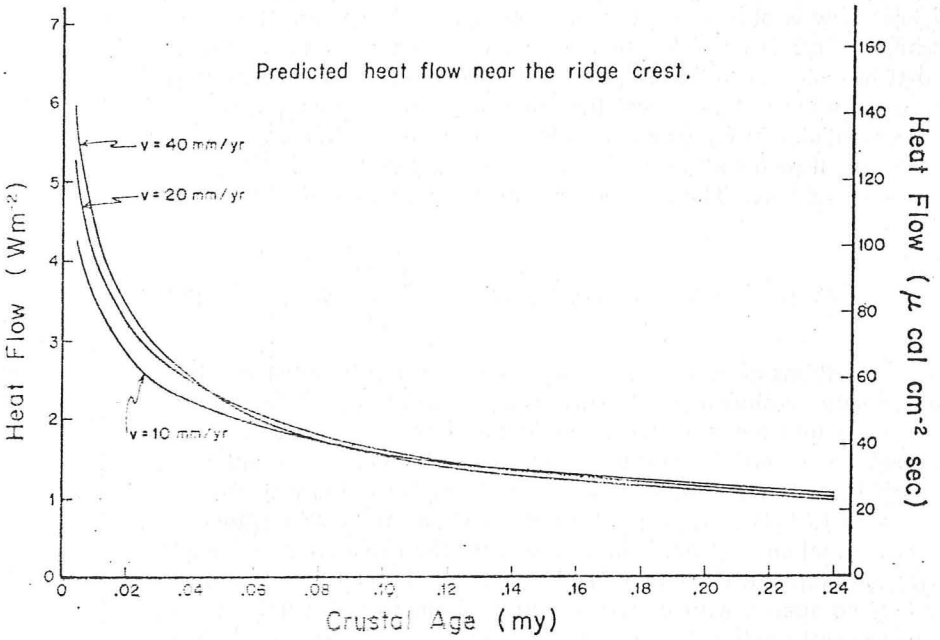

FIG. 4(a). Predicted heat flow near the ridge crest for three spreading velocities

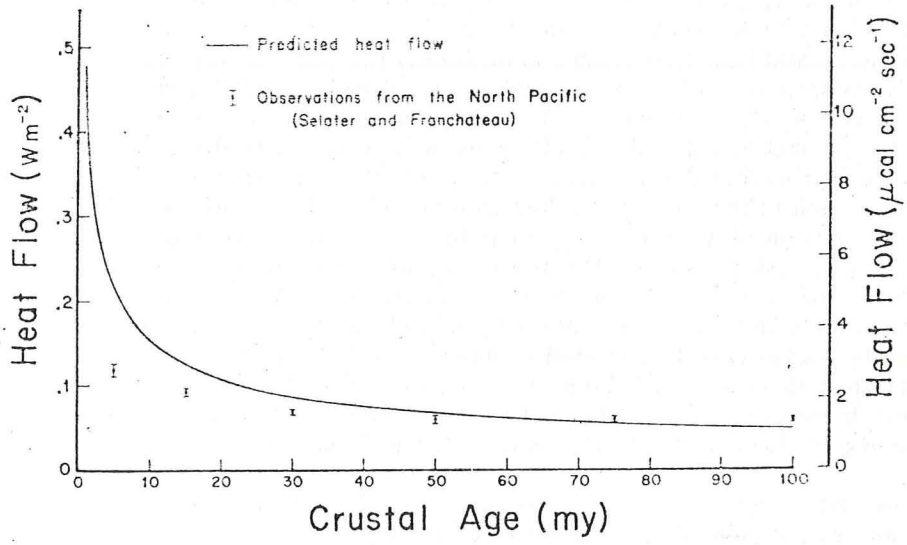

FIG. 4(b). Predicted heat flow and observations from the North Pacific (observations from Sclater & Francheteau 1970).

and observed elevation everywhere except at the ridge crest where the misfit is 256 m.

The predicted heat flow is also strongly dependent upon lithospheric thickness. The inverse relationship between the length of the intrusion zone and spreading velocity requires that in faster spreading ridges the melting temperature isotherm is closer to the surface, resulting in higher heat flow than for slower spreading ridges. However, at distances sufficiently far from the ridge crest such that the asymptotic solution is valid, the heat flow for all ridges is a function only of crustal age and is independent of spreading velocity. The asymptotic expression is easily obtained from equation (14)

$$\text{Heat flow} = k\partial_z T = 4{\cdot}22\times 10^{-3}\, T_m\, T_w \sqrt{\left(\frac{k\rho c_p}{t}\right)}\ \text{W m}^{-2} = \frac{0{\cdot}476}{\sqrt{t}}\ \text{W m}^{-2} \qquad (20)$$

where t is measured in millions of years. The heat flow near the ridge crest for three different spreading velocities is shown in Fig. 4(a). We present the heat flow only for crustal ages greater than 0·01 My since an analytic solution valid at the junction between the intrusion zone and the surface shows that the heat flow suffers a logarithmic singularity there.* The values are considerably higher than most observations but there is reason to believe that an alternate mechanism of heat transport, resulting from hydrothermal circulation, is important near the ridge crest and might be responsible for this discrepancy (Lister 1972). The asymptotic heat flow calculated from equation (20) is compared with empirical results from the North Pacific in Fig. 4(b). Again, the model predicts higher heat flow than existing observations, at least for the first 30 My, but this discrepancy may not reflect too unfavourably upon the model. Heat flow observations tend to be biased toward low values because probes are often put into sediment ponds surrounded by significant topography (LePichon & Langseth 1969), the probes are not exactly vertical when inserted, and there are possible effects of hydrothermal circulation. In addition, the error bars in Fig. 4(b) represent the standard deviation of the mean of the heat flow observations which is considerably smaller (by factors of 2–5) than the standard deviations of the heat flow observations themselves. We conclude that the model provides a moderately acceptable fit to the empirical heat flow results, nevertheless, the effect of varying some of the physical parameters to obtain closer agreement will be considered later.

Although gravity is generally considered to be a moderately insensitive determinator of geophysical quantities, it still provides a useful test of the model. A gravitational anomaly measured at the sea surface may result from mass anomalies supported by finite strength of the lithosphere, fluid motions below the lithosphere, and/or a horizontal variation of vertical composition in an isostatically balanced lithosphere–asthenosphere system. We shall consider only the latter contribution. If the depth of the crest below sea level is known, the geometry of the ridge is completely specified and the free air gravitational anomaly can be efficiently calculated by a method proposed by Parker (1973). The results, presented in Fig. 5(a) for three spreading velocities, show that the predicted free air gravitational anomaly is positive over the ridge crest, becomes slightly negative a few hundred kilometres onto the flank, and that the magnitude of the total anomaly decreases with increasing spreading rate.

If the density difference, $\Delta\rho = \bar{\rho}_L - \rho_A$, is caused by thermal contraction in the lithosphere, then an average value of the coefficient of volume expansion, α_v, for lithospheric rocks can be obtained from

$$\Delta\rho(x) = \frac{1}{Z(x)} \int_0^{Z(x)} \rho_0\, \alpha_v\, T(x, y)\, dy \qquad (21)$$

* The author is grateful to Dr N. Sleep for pointing this out.

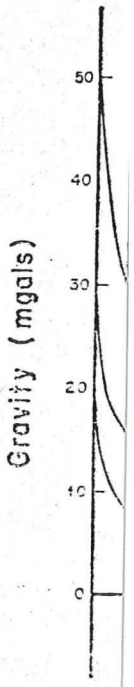

FIG. 5(

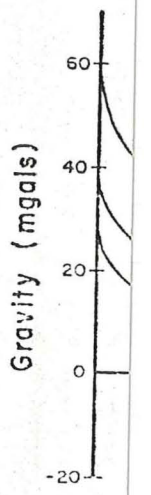

FIG. 5(b)

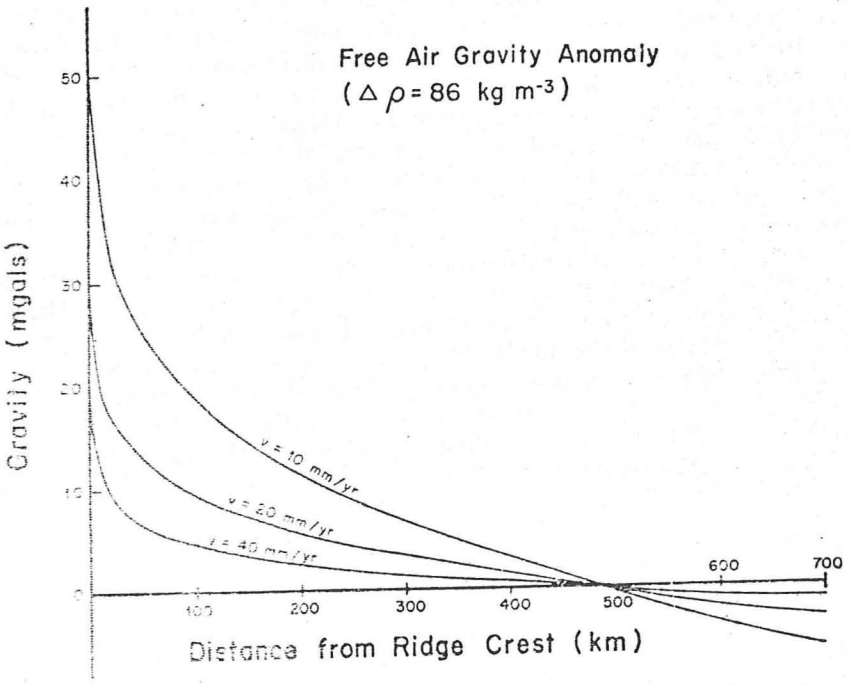

FIG. 5(a). Predicted free-air gravity anomaly calculated with $\Delta\rho = 86\,\mathrm{kg\,m^{-3}}$.

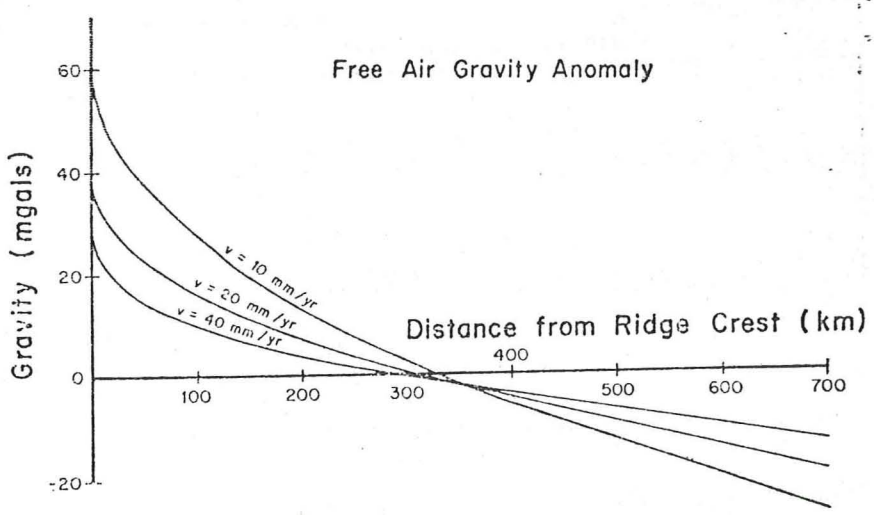

FIG. 5(b). Predicted free-air gravity anomaly using five layers and a coefficient of volume expansion of $3{\cdot}86/^{\circ}\mathrm{C}$.

where $Z(x)$ is the lithospheric thickness at a distance x. Substituting the asymptotic temperature from equation (14), and setting $\Delta\rho = 86\,\mathrm{kg\,m^{-3}}$ we obtain

$$\alpha_v = 3{\cdot}8 \times 10^{-5}/^{\circ}\mathrm{C}.$$

This is a value frequently used for lithospheric rocks (McKenzie 1967).

Alternatively, this coefficient of volume expansion, with the known temperature distribution, can be used to calculate the density everywhere in the lithosphere, and hence, refinement of the gravity calculation can be obtained by integrating the resultant density structure. In practice, the lithosphere was divided into layers whose top and bottom surfaces were isotherms, and each layer was ascribed an average density depending upon its temperature distribution. Usually five to seven layers were required before the gravitational anomaly, calculated by summing the contributions of each layer, had converged. The free air gravity anomalies for three spreading velocities are shown in Fig. 5(b). The anomalies are enhanced compared to those in Fig. 5(a) because this method concentrates the high density material near the surface.

Free-air gravity observations from the mid-Atlantic ridge and the East Pacific Rise (redrawn from Talwani, LePichon & Ewing 1965) are shown in Fig. 6. The inverse relationship between amplitude of the anomaly and spreading rate is apparent despite the rough topography of the mid-Atlantic. The dashed line represents the free air anomaly predicted by the model using the above coefficient of expansion. We have used a spreading velocity of 44 mm/year for the East Pacific Rise and a value of 13 mm/year for the mid-Atlantic (Pitman & Talwani 1971). The gravity calculated from the model appears as an acceptable fit to a smoothed version of the observations,

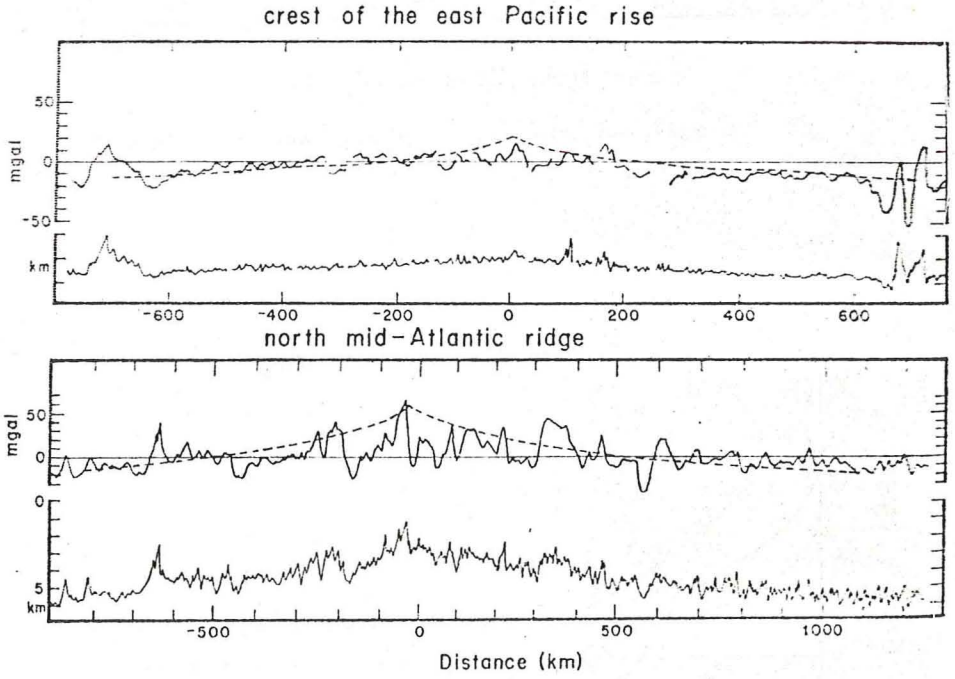

FIG. 6(a). Free-air gravity anomaly over the mid-Atlantic ridge from Talwani *et al.* (1965) with predicted anomaly from the model for a spreading rate of 13 mm/yr.

FIG. 6(b). Free-air gravity anomaly over the East Pacific Rise from Talwani *et al.* (1965) with predicted anomaly from the model for a spreading rate of 44 mm/yr.

although the observed anomaly over the East Pacific Rise does not exhibit the peak predicted by the model. Additional observational evidence of the existence of a positive free-air gravity anomaly over ridges is given by Kahle & Talwani (1973). Using $1° \times 1°$ averages in the Indian Ocean, they showed that ridges there are associated with positive anomalies of 20–50 mgal.

A laboratory test of the model

The wax model of Oldenburg & Brune (1972, 1975) has been used primarily to understand the development of the orthogonal ridge transform fault pattern which characterizes oceanic spreading centres. However, this model also shows that the solid plate continually thickens with increasing distance from the ridge crest; and indeed efforts to explain this phenomenon resulted in the physical model by Parker & Oldenburg (1973). There are two differences between the wax model and the Earth: the first is the concept of an intrusion zone, which exists in the Earth, but not in the wax since the melting temperature isotherm intersects the surface. This introduces the second difference; the top of the lithosphere is approximately at a constant temperature, while in the laboratory model, the surface temperature must decrease from the melting temperature at the ridge crest to some value on the flanks determined by the rate of surface cooling. The lack of an intrusion zone is probably unimportant in affecting the thickness of the solid plate at distances greater than a fraction of a centimetre from the crest, but the non-constancy of surface temperature may be important. Nevertheless, the wax model offers a rare opportunity to test a prediction of a theoretical model, and we shall compare the measured thickness of the solid plate with that predicted by equation (16).

Under conditions of constant rates of spreading and surface cooling, the wax was allowed to spread symmetrically until plates $\sim 0{\cdot}2$ m in length were formed; the plates were then lifted out of the wax and the thickness measured with a microscope. All of the samples taken under these controlled conditions were consistent with a thickening

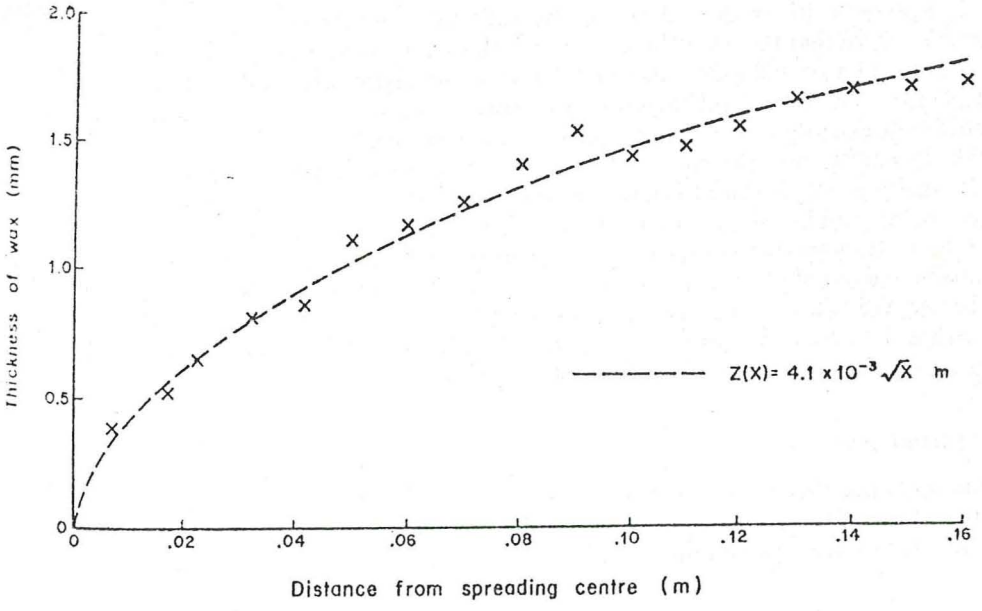

FIG. 7. Measured thickness of the wax plate.

proportional to the square root of distance from the ridge crest, although the constant of proportionality varied by up to 25 per cent, depending upon rates of spreading and surface cooling. A representative thickness profile is shown in Fig. 7.

The values of $H = L/c_p(T_m - T_s)$, where T_s is the surface temperature, must be known before equation (16) can be applied. The surface temperature was recorded with an infrared scanning device (Texas Instrument Thermoscope #700) which measures the temperature of the equivalent blackbody source. The true surface temperature, obtained by correcting the blackbody temperature for the finite skin depth of the wax remained approximately 10 °C below the melting temperature at distances greater than 10 mm from the ridge. With $L = 2{\cdot}2 \times 10^5$ J kg^{-1}, $c_p = 2{\cdot}9 \times 10^3$ J kg^{-1} °C^{-1}, $k = 2{\cdot}5$ W m^{-1} °C^{-1} and $\rho = 8{\cdot}7 \times 10^2$ kg m^{-3}, we obtain $H = 7{\cdot}6$ and $\alpha = 0{\cdot}25$. The half-rate spreading velocity was $1{\cdot}5 \times 10^{-3}$ m s^{-1} so the predicted theoretical thickness is $Z(x) = 4{\cdot}1 \times 10^{-3} \sqrt{(x)}$ m. In view of possible uncertainties in the values of the physical constants, errors in reading the thermograms and in carrying out the experiment, we judge this predicted value to be in good agreement with the experimentally measured value of $Z(x) = 5{\cdot}2 \times 10^{-3} \sqrt{(x)}$ m.

Modifications of the model

The numerical results have shown that this physical model predicts ridge elevation, heat flow, and gravity in reasonable agreement with observations, and yet there are serious criticisms which must be considered before the model can be representative of the Earth. It is generally agreed that the seismic low velocity zone, which we shall equate to the asthenosphere, cannot be accounted for by temperature gradients alone (Anderson & Sammis 1970), and the most acceptable hypothesis is that the asthenosphere is a zone of partial melt. However, this region cannot be completely molten, as we have assumed in the numerical model, or no shear waves would be transmitted at all. Unfortunately, the percentage and distribution of partial melt is not known. Petrologists require high values (~30 per cent) beneath the ridge crests in order to explain the observed composition of rocks dredged from the sea floor (Kay, Hubbard & Gast 1970). This is consistent with seismic evidence which shows that S_n phases are not seen to propagate across oceanic ridges (Molnar & Oliver 1969) and that shear waves propagating parallel to or across an oceanic ridge suffer high attenuation (Solomon 1973). The average value of partial melt throughout the low velocity zone is probably considerably lower than the value beneath the ridge crests. Anderson *et al.* (1971) have shown that the low velocity zone for shear waves can be explained by an asthenosphere with a partial melt value of 1–10 per cent, depending on the aspect ratio of the partial melt zones, and therefore a reasonable estimate for the average value of partial melt existing in the asthenosphere is a few per cent.

In addition to considering the effects of varying the amount of partial melt we must allow the melting temperature to change with depth, and also consider the effect of heat sources other than latent heat, on the heat budget which determines the growth of the lithosphere. Radioactive matter in the lithosphere and temperature gradients in an asthenosphere composed of a variety of chemical species are potentially important heat sources. We will later discuss in detail the region near the ridge crest, but for the present we shall concern ourselves only with the effects of these modifications to the model on the global growth of the lithospheric plate.

(a) *Effect of partial melt*

A partially molten asthenosphere is easily incorporated into the model by multiplying the latent heat of fusion, or equivalently H, by the percentage of partial melt. The effect of this is to increase α and therefore increase the plate thickness via equation

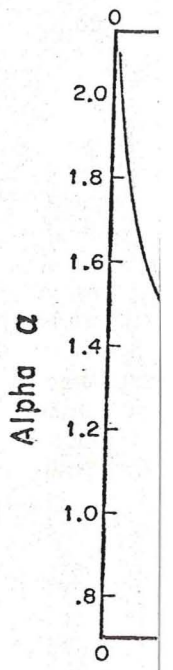

(18). The relationship
here is shown in Fig. 8.
melt changes by two o
value of H, there alway
the topography. Also, t
in $\Delta\rho$ and hence the pr
surface heat flow is ins
decrease from 100 to 1
clusion therefore is that
perhaps slightly better th
partial melt. The two p
partial melt are the thick
to calculate the elevation
5 per cent partial melt p
this is considerably deep
velocity zone (Dziewons
sphere at a crustal age
beneath the plate must e
coefficient of volume exp
and therefore $\Delta\rho$ must
partial melt of at least 3
using heat derived only f
observations. If it is u
lithosphere, then additio

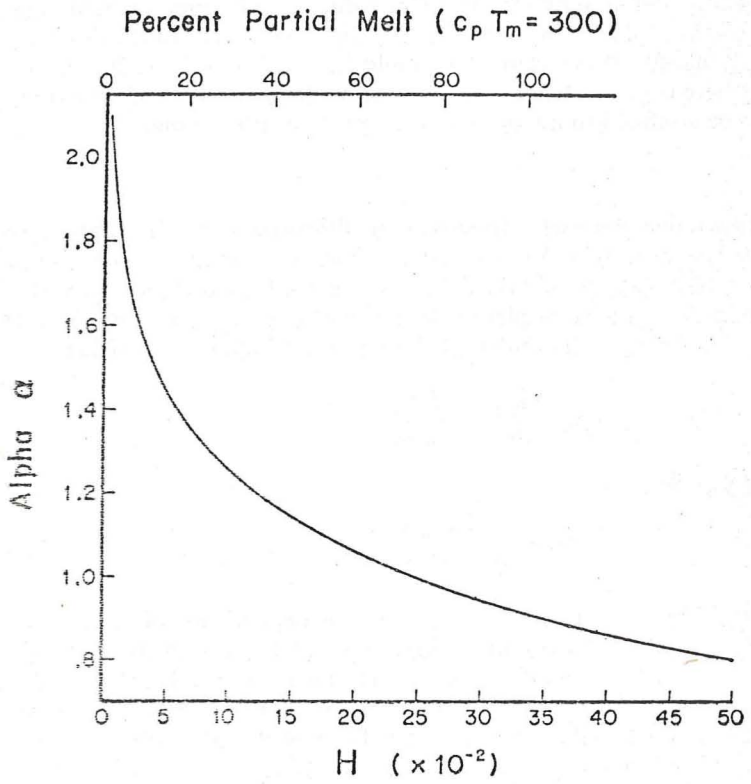

FIG. 8. Relationship between α and H.

(18). The relationship between α and H for the range of physical parameters used here is shown in Fig. 8. Importantly, α varies by only a factor of 2 while the partial melt changes by two orders of magnitude. Since the plate thickens as $\sqrt{t}$ for each value of H, there always exists a value of $\Delta\rho$ such that an excellent fit can be made to the topography. Also, the increased thickness is balanced by a corresponding decrease in $\Delta\rho$ and hence the predicted free air gravity anomaly is not greatly changed. The surface heat flow is insensitive to a reduction in the amount of partial melt, and a decrease from 100 to 1 per cent lowers the heat flow by only 23 per cent. The conclusion therefore is that topography, heat flow, and gravity can be fit as well, and perhaps slightly better than in the numerical example by allowing smaller amounts of partial melt. The two primary constraints to allowing arbitrarily small amounts of partial melt are the thickness of the lithosphere and the relationship between $\Delta\rho$ used to calculate the elevation and α_v, the coefficient of volume expansion. For example, a 5 per cent partial melt predicts a thickness of 178 km at a crustal age of 100 My and this is considerably deeper than the lid of 90–120 km predicted by models for the low velocity zone (Dziewonski 1971). If the maximum allowable thickness for the lithosphere at a crustal age of 100 My is 130 km, then the percentage of partial melt beneath the plate must exceed 30 per cent (see Fig. 8). Also, a lower bound for the coefficient of volume expansion for lithospheric rocks is $\sim 2{\cdot}5 \times 10^{-5}/°C$ (Clark 1966) and therefore $\Delta\rho$ must be greater than $62\,kg\,m^{-3}$ again requiring a percentage of partial melt of at least 30 per cent. This is approximately the limit to which a model using heat derived only from latent heat can be pushed and still satisfy the geophysical observations. If it is unacceptable to have such large values of melt beneath the lithosphere, then additional modifications to the model are required.

The value of $\Delta\rho = 87\,\mathrm{kg\,m^{-3}}$ found in the numerical example provides a constraint to the physical model in another way. This value was obtained by assuming a completely molten asthenosphere. Since the density difference between the liquid and solid phases is likely about 10 per cent, $\Delta\rho$ should have been at least $300\,\mathrm{kg\,m^{-3}}$. Hence, if the lithosphere is grown from a material with a large amount of partial melt then this melt must be confined to a fairly narrow zone beneath the plate.

(b) *Radioactivity*

The effect of radioactive material is to reduce the thickness of the lithosphere and to increase the surface heat flow by a small amount. An approximation to the asymptotic equation (20), may be obtained by assuming a heat budget in a vertical column. If the thickness of the solid plate is $h(t)$ at a distance $x = vt$ from the ridge crest, then the heat budget, with the differential equation $d^2T/dz^2 = 0$, yields

$$\rho L \frac{dh(t)}{dt} = \frac{kT_m}{h(t)}$$

which can be integrated to give

$$h(t) = \sqrt{\frac{2kT_m t}{\rho L}}. \tag{22}$$

Importantly, this formulation still yields a square root dependence of thickness on time. The thicknesses predicted by equation (22) are about 30 per cent too large when compared to the correct solution, but if L is replaced by an artificial value, $\tilde{L} = L/2H\alpha^2$ then equation (22) is exact. (Since $2H\alpha^2 \to 1$ for larger H, the discrepancy between these two formulations is reduced as H increases.) To treat the effect of radioactivity added to a lithosphere grown from a partial melt, we assume a vertical heat budget with the pseudovalue of latent heat. Since the radioactivity is distributed throughout, the assumption that the heat from this source flows vertically is very good. The heat budget equation becomes

$$\rho\tilde{L}\frac{dh(t)}{dt} + qh(t) = k\frac{\partial T}{\partial z} \tag{23}$$

where q is the radioactive concentration $q\,\mathrm{W\,m^{-3}}$. From the one-dimension steady-state equation for temperature, $d^2T/dz^2 = -(q/k)$, and the boundary conditions $T(t, 0) = 0$ and $T(t, h(t)) = T_m$ we obtain

$$\frac{dh(t)}{dt} = \frac{1}{\rho\tilde{L}}\left\{\frac{T_m k}{h(t)} - \frac{q}{2}h(t)\right\}$$

and

$$h^2(t) = \frac{2kT_m}{q}\left(1 - \exp\left(-qt/\rho\tilde{L}\right)\right). \tag{24}$$

The thickness of the lithosphere at a crustal age of 100 My for different values of radioactivity and partial melt is given in Fig. 9. The effect of radioactivity is to reduce the thickness by only moderate amounts; for example, a crustal thickness of 120 km is thinned by about 8 km with a radioactive concentration of $1{\cdot}25 \times 10^{-7}\,\mathrm{W\,m^{-3}}$ ($0{\cdot}3 \times 10^{-13}\,\mathrm{cal\,cm^{-3}\,s^{-1}}$). Radioactivity will also increase the heat flow at the surface by an amount $qh(t)/2$ and hence, a value of $8{\cdot}4 \times 10^{-8}\,\mathrm{W\,m^{-3}}$ for a 100 km thick lithosphere will increase the heat flow by about $4{\cdot}2 \times 10^{-3}\,\mathrm{W\,m^{-3}}$ ($0{\cdot}1\,\mu\mathrm{cal\,cm^{-2}\,s^{-1}}$).

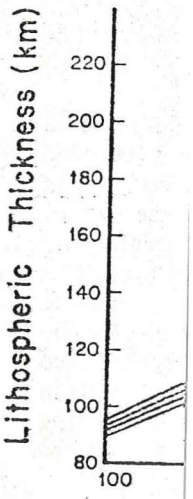

FIG. 9.

(c) *Effect of thermal*

The assumptions
that the asthenosphe
temperature led us t
determined by the h
and attached to the
asthenosphere compo
temperatures, and he
In addition, the melt
Ito & Kennedy (1967
possible mantle rock.
thermal gradient mu
molten. Further con
sphere arise if a sma
small percentage of th
(Wyllie 1971). These
exist in a partially m
be included in the he

Let us assume tha
$T_m(z) = T_{m_0} + \gamma z$ whe
also assume that the
ordinate and has the
bottom of the slab is

and this can be put in

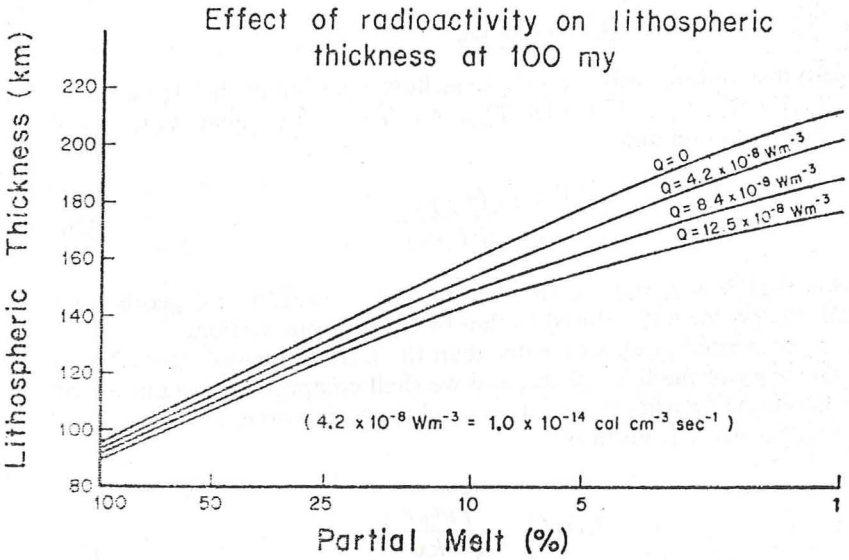

FIG. 9. Effect of radioactity on lithospheric thickness at 100 My.

c) Effect of thermal gradients in the asthenosphere

The assumptions that the melting temperature was independent of pressure and that the asthenosphere was composed of a single chemical species at the melting temperature led us to the conclusion that the rate of growth of the lithosphere was determined by the heat of fusion released when partially molten material solidified and attached to the underside of the plate. A more realistic model must allow an asthenosphere composed of a variety of mineral assemblages with different melting temperatures, and hence permit a range of temperatures over which melting can occur. In addition, the melting temperature of dry rocks increases with increasing pressure. Ito & Kennedy (1967) have shown that the melting temperature of dry peridotite, a possible mantle rock, increases by approximately $3\,^{\circ}\mathrm{C\,km^{-1}}$, and therefore the geothermal gradient must be at least as large if the asthenosphere is to be partially molten. Further complications to the possible temperature structure in the asthenosphere arise if a small amount of water is present, for then (incipient) melting of a small percentage of the rock may occur substantially below the dry solidus temperature (Wyllie 1971). These considerations suggest that substantial thermal gradients may exist in a partially molten asthenosphere and the associated heat flux must therefore be included in the heat budget for the growth of the lithosphere.

Let us assume that the variation of melting temperature with depth has the form $T_m(z) = T_{m_0} + \gamma z$ where T_{m_0} is the melting temperature at the surface, $z = 0$. We shall also assume that the geotherm in the asthenosphere is independent of the x coordinate and has the form $T(x, z) = T_{m_0} + \beta z$. The heat budget equation at the bottom of the slab is

$$-\hat{n}.\hat{z}k\beta + \hat{n}.\hat{x}\rho vL = -k\frac{\partial T}{\partial n}$$

and this can be put into a first order differential equation (see Appendix B)

$$\frac{dZ(x)}{dx} = \frac{(\partial T/\partial z) - \beta}{(\rho vL/k) + (\partial T/\partial x)} \qquad (25)$$

which must be solved simultaneously with the heat flow equation in the slab and the condition $T(x, Z(x)) = T_{m_0} + \gamma z$. If we let $T(x, z) = \tilde{T}(x, z) + \gamma z$ then $\tilde{T}(x, z)$ still satisfies the heat flow equation and

$$\frac{dZ(x)}{dx} = \frac{(\partial \tilde{T}/\partial z) + (\gamma - \beta)}{(\rho v L/k) + (\partial \tilde{T}/\partial x)}. \tag{26}$$

In the special case that $\beta = \gamma$, that is, the melting point gradient and geothermal gradient are equal, the problem is reduced to that of the previous section.

The effect of a geothermal gradient greater than the melting temperature ($\beta > \gamma$) is to reduce the thickness of the lithosphere, and we shall compute the magnitude of this thinning as a function of β when $\gamma = 0$. To a good approximation, the temperature distribution in the lithosphere is given by

$$\tilde{T}(x, z) = \frac{T_m \, erf\left(\frac{z}{2}\sqrt{\frac{\rho c_p v}{kx}}\right)}{erf\left(\frac{Z(x)}{2}\sqrt{\frac{\rho c_p v}{kx}}\right)}. \tag{27}$$

With this temperature distribution, equation (26) can be integrated to find $Z(x)$. Fig. 10 shows the resulting thickness of the lithosphere at a crustal age of 100 My as a function of percentage of partial melt when gradients up to $\beta = 3°\,\mathrm{C\,km^{-1}}$ exist. For large amounts of melt, 50–100 per cent, these gradients reduce the thickness by only a few kilometres, while for a 10 per cent melt a gradient of $2\,°\mathrm{C\,km^{-1}}$ thins the lithosphere by 30 km. The solution for $Z(x)$ and the temperature distribution above do not solve the heat flow equation exactly, and the dashed lines in Fig. 10 indicate

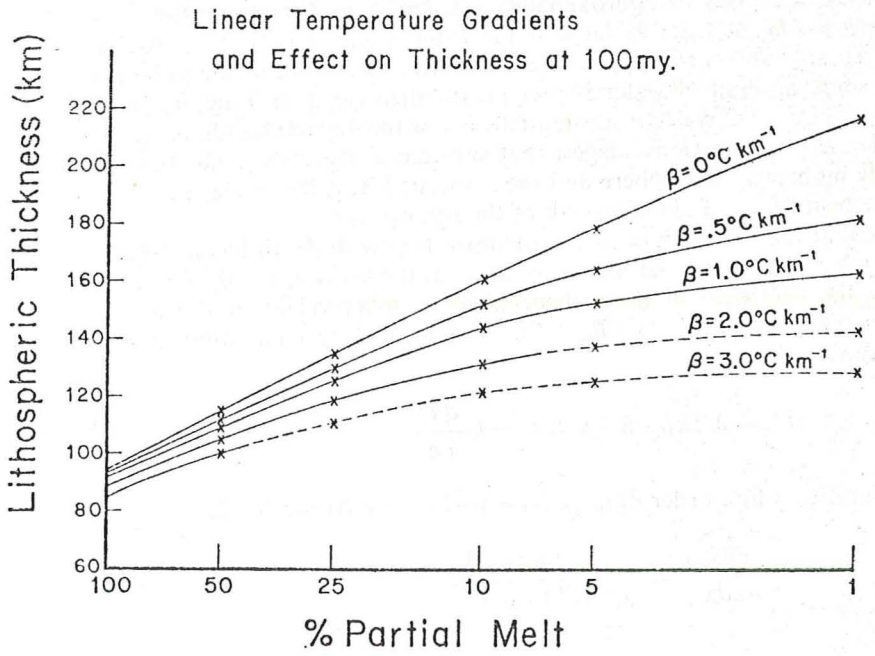

FIG. 10. Effect of linear temperature gradients on lithospheric thickness at 100 My.

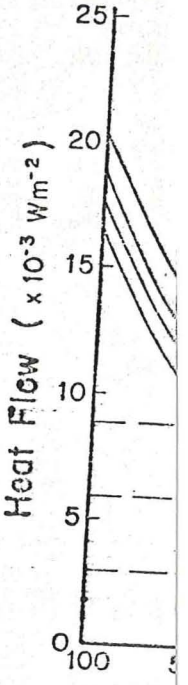

FIG. 11. Relati
of fu

where the solution m
errors in solving that
dashed lines provide
temperature gradients
100 My is 134 km an
100 My is $8{\cdot}8 \times 10^{-3}$
$\beta = 3{\cdot}0$, for which the
melt.

In Fig. 11 we hav
bottom of the lithosph
then the latent heat don
of melt, ~1 per cent, th
temperature gradients.

The existence of ter
major factor in determ
partial melt are small.
produced under conditi
geophysical observation
$3\,°\mathrm{C\,km^{-1}}$ and values o
as well as empirical obse
$\Delta\rho$ used to calculate th
expansion are also listed
is moderately good and p
Near the ridge crest, 0–
decreases. We shall disc

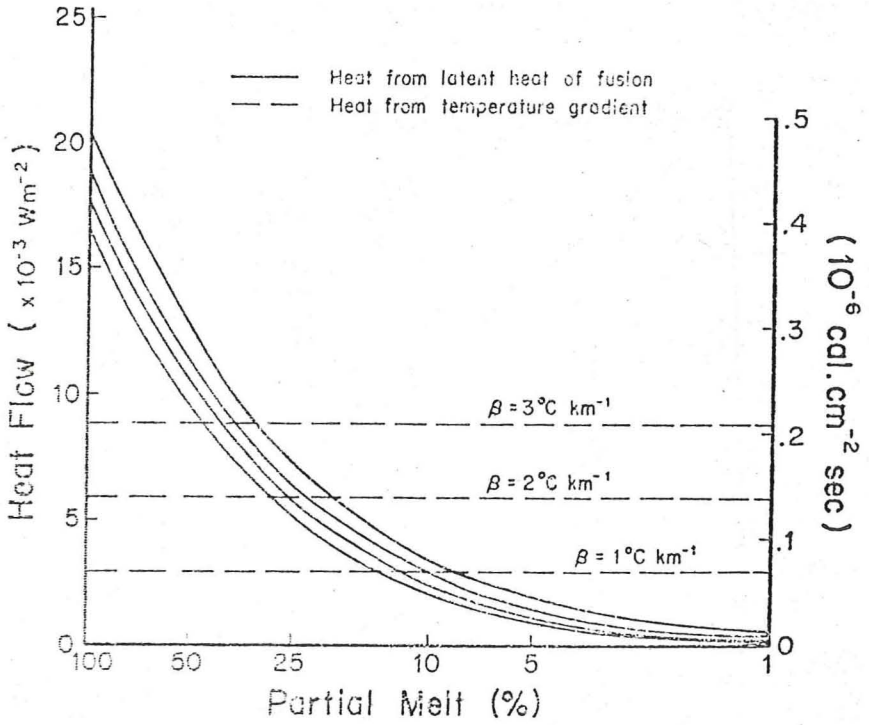

FIG. 11. Relative contributions to the heat budget of the slab from the latent heat of fusion and from thermal gradients in the asthenosphere.

where the solution may not be reliable because of reasonably large, (~10 per cent), errors in solving that equation. Nevertheless, there is reason to believe that even the dashed lines provide a good indication of the amount of thinning caused by linear temperature gradients. With 25 per cent melt and $\beta = 0$, the thickness of the slab at 100 My is 134 km and the average heat flow into the base of the slab from 40 to 100 My is $8{\cdot}8 \times 10^{-3}$ W m^{-2} but this is the same heat flow as that obtained from $\beta = 3{\cdot}0$, for which the solution in Fig. 10 gives a thickness of 128 km for a 1 per cent melt.

In Fig. 11 we have plotted the relative contributions to the heat flow into the bottom of the lithosphere. If the percentage of partial melt is high, >50 per cent, then the latent heat dominates the heat flow into the slab, while for very small amounts of melt, ~1 per cent, the latent heat released is negligible compared to that from small temperature gradients.

The existence of temperature gradients in the asthenosphere may therefore be a major factor in determining the rate of growth of the lithosphere if the amounts of partial melt are small. In order to compare the predictions from lithospheric slabs produced under conditions of linear temperature gradients in the asthenosphere with geophysical observations, we shall consider the effect of a temperature gradient of 3 °C km^{-1} and values of partial melt from 100 to 1 per cent. The predicted elevations as well as empirical observations from the Pacific are shown in Fig. 12. The values of $\Delta\rho$ used to calculate the elevation and the corresponding coefficients of volume expansion are also listed there. For crustal ages between 2 and 80 My the agreement is moderately good and perhaps not significantly different for all values of partial melt. Near the ridge crest, 0–2 My, the agreement worsens as the amount of partial melt decreases. We shall discuss this discrepancy later, but for now appeal to the con-

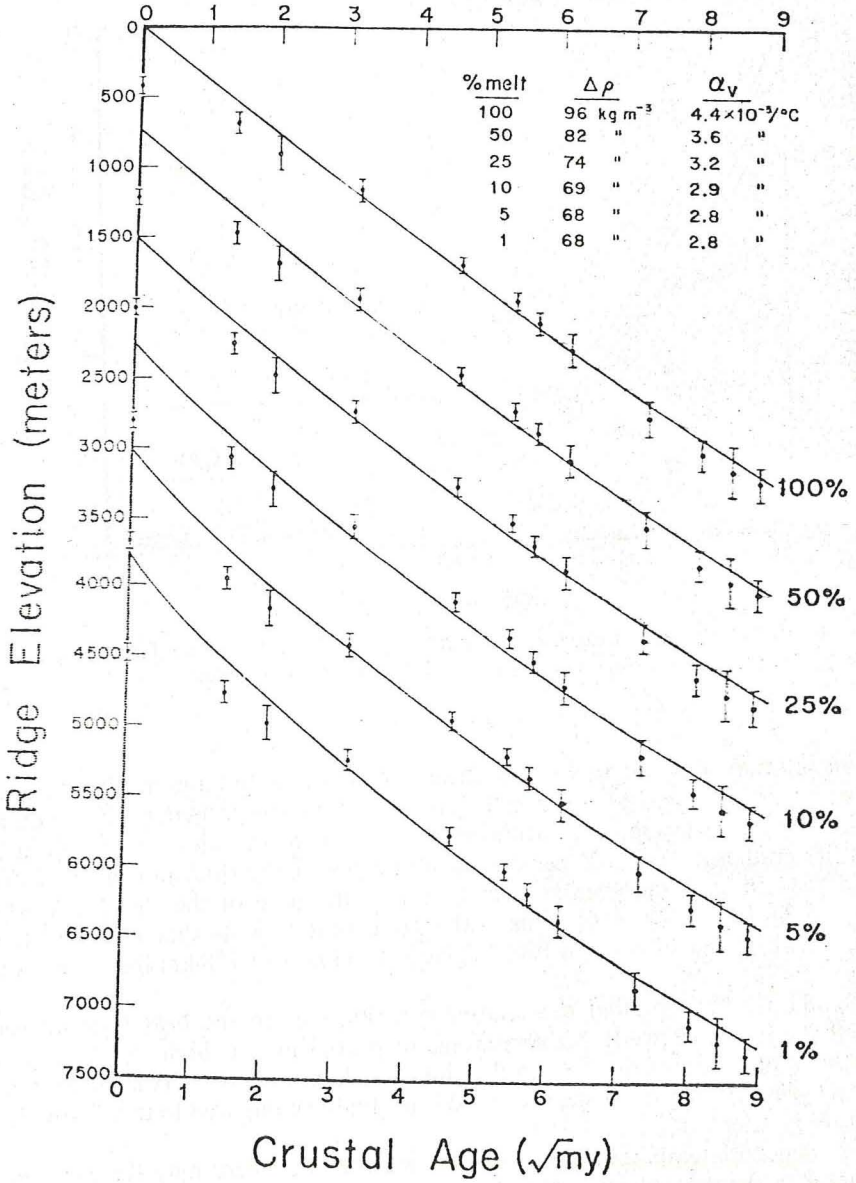

FIG. 12. Predicted elevations from lithospheres evolved under conditions of various amounts of partial melt and a temperature gradient of 3°C/km in the asthenosphere. The profiles with the empirical observations from the North Pacific (Sclater *et al.* 1971) have been stacked for viewing purposes and the absolute value of the depth is not meaningful.

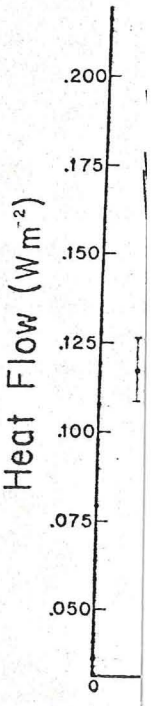

FIG. 13. amounts sphere.

clusions of Da anomalously lo flow as well as fractions of mel and the values important conc a trade-off exis temperature gra increased gradi

Near the ridge c

Both seismic the ridge crest, heat of fusion, a the solution to equations (6) to shape of the un partial melt will or time average the magma cool

The true rela

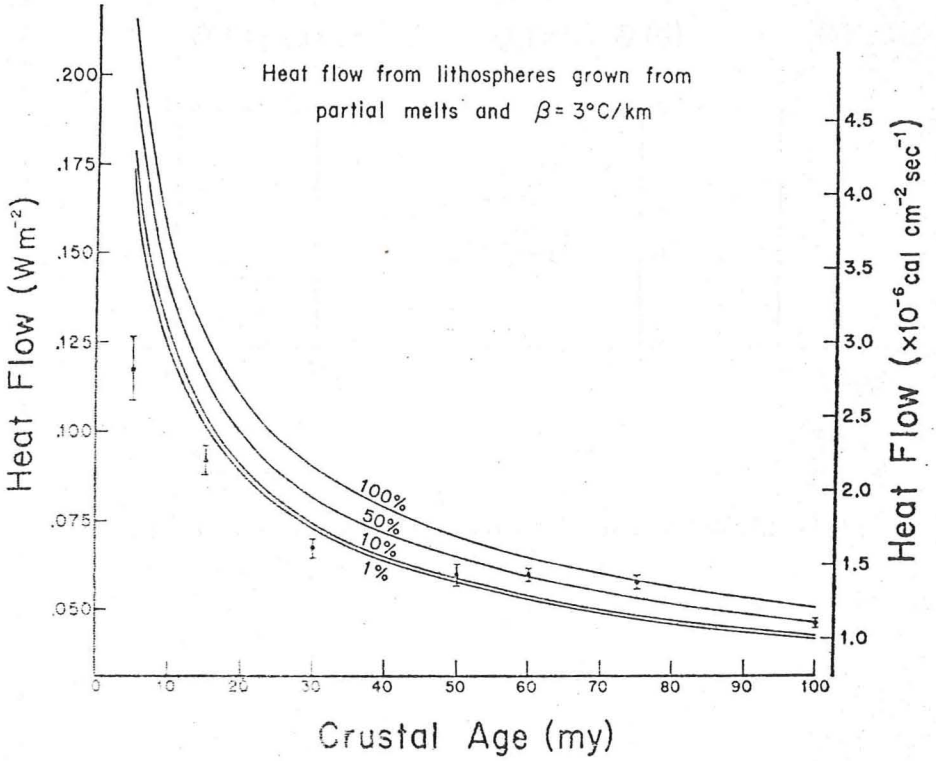

FIG. 13. Predicted heat flow from lithospheres evolved under conditions of various amounts of partial melt and a temperature gradient of 3°C/km in the asthenosphere. The empirical observations for the North Pacific have been taken from Sclater & Francheteau 1970.

clusions of Davis & Lister (1974) that the elevation near the ridge crest may be anomalously low when compared to the whole elevation profile. The predicted heat flow as well as observations from the North Pacific are shown in Fig. 13. For low fractions of melt, the heat flow is decreased slightly from that in the numerical example and the values of α_v all fall within acceptable bounds. These results suggest an important conclusion: in the heat budget determining the growth of the lithosphere, a trade-off exists between the heat derived from latent heat and that obtained from temperature gradients, and a decrease in the melt fraction can be counteracted with increased gradients to produce a lithosphere which satisfies geophysical observations.

Near the ridge crest

Both seismic and petrologic studies require large amounts of partial melt beneath the ridge crest, thus the major heat source is most likely that derived from the latent heat of fusion, and the growth of the lithosphere in this region should be explained by the solution to the equations of the physical model. Full solutions to the set of equations (6) to find u, the temperature distribution along the vertical wall, and the shape of the underside of the lithosphere for H corresponding to different values of partial melt will be found. Also, different relationships between $\overline{T}(z)$, the steady state or time averaged temperature distribution, and $T_f(z)$, the final temperature to which the magma cools before the next episode of intrusion, will be discussed.

The true relationship between $\overline{T}(z)$ and $T_f(z)$ is not known but is likely dependent

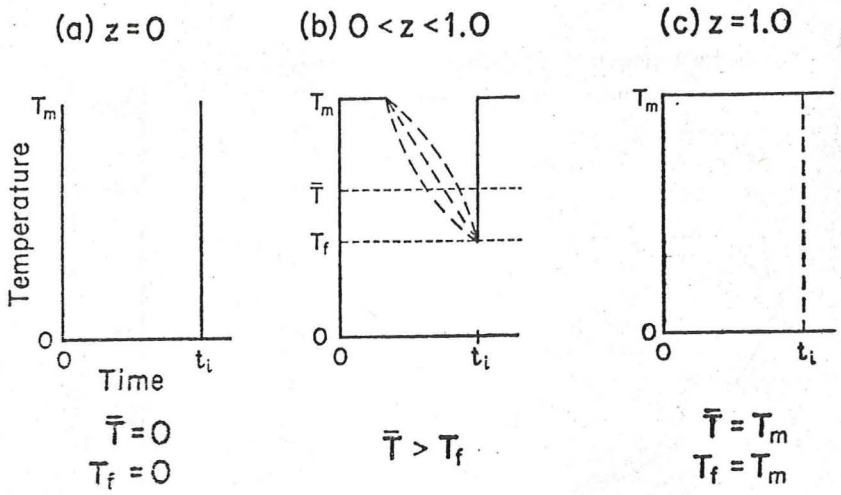

FIG. 14. Relationship between $\bar{T}$ and T_f along the intrusion zone.

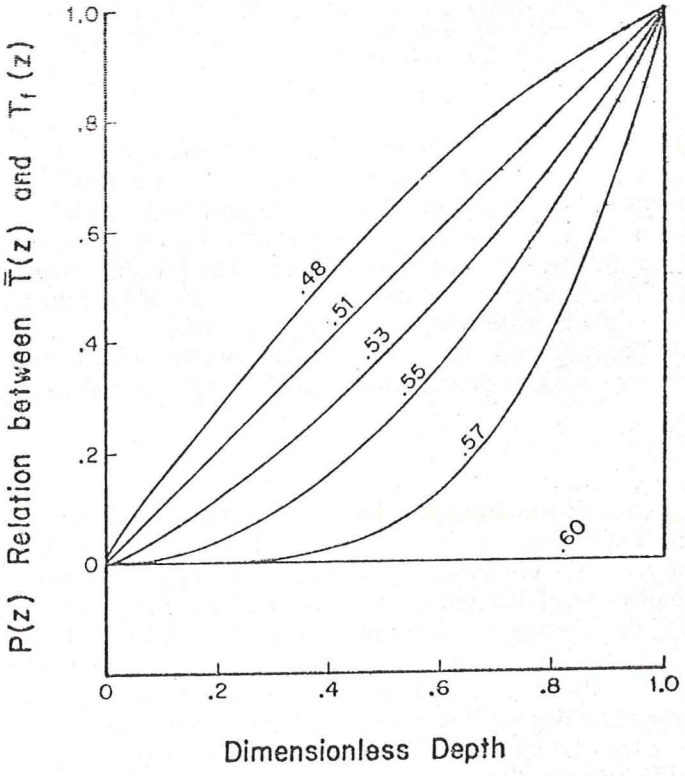

FIG. 15. Six arbitrary curves for $P(z)$ and the resulting values of u.

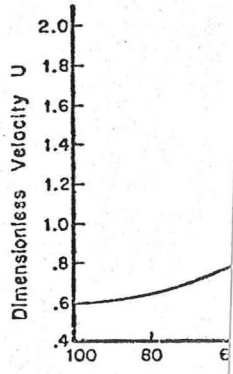

upon the spatial d
intrusion episodes.
to one of the diagr

with $0 \leqslant P(z) <$
instantaneously to
its melting point a
fication requires t

Fig. 15 shows six
the physical const
to reduce u sligh
temperature distr
shown in Fig. 16
the ridge crest is

The effect of
lengthen the intr
crest. The tempe
between u and th
the lithosphere is
to the amount of

Conclusions

In an effort t
that the predicte
the ridge crest.

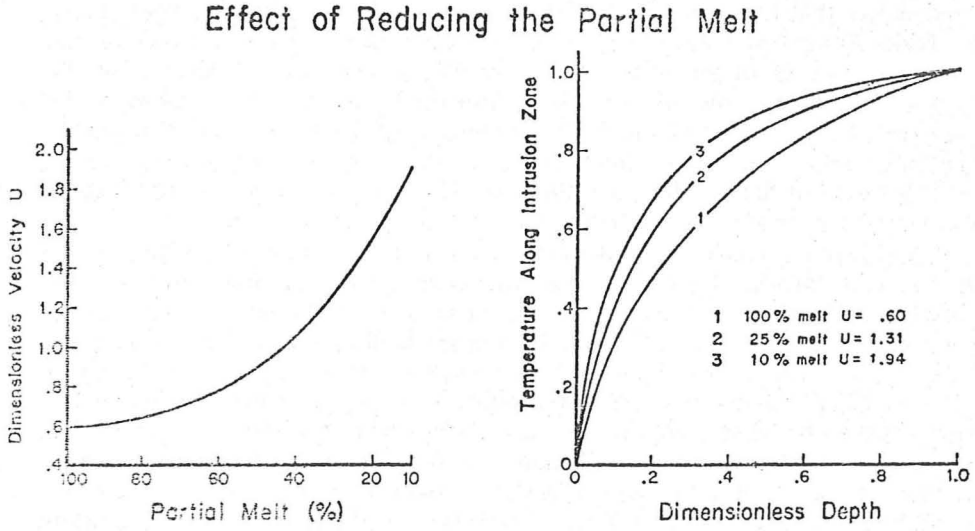

FIG. 16. Effect of reducing the percentage of partial melt.

upon the spatial distribution of dike injection, spreading velocity, and time between intrusion episodes. At each depth z the relationship between $\bar{T}$ and T_f will be similar to one of the diagrams in Fig. 14. We shall model the relationship as

$$\bar{T}(z) = T_f(z) + P(z)\big(T_m(z) - T_f(z)\big) \tag{28}$$

with $0 \leqslant P(z) < 1{\cdot}0$ so that if $P(z) = 0$ the injected material is assumed to cool instantaneously to its final temperature, while if $P(z) = 1$, the material is always at its melting point and hence the injection process proceeds continuously. This modification requires that equation (6) be replaced by

$$-\frac{\partial \bar{T}}{\partial x} = 2u\left\{H + \frac{1}{1-P(z)}\left(1-\bar{T}(z)\right)\right\}. \tag{29}$$

Fig. 15 shows six arbitrary curves for $P(z)$ and the resulting value of u. The values of the physical constants are those used in the numerical model. The effect of $P(z) > 0$ is to reduce u slightly or equivalently, to reduce the length of the intrusion zone. The temperature distributions on the vertical wall are not significantly changed from that shown in Fig. 16 for 100 per cent melt and $P(z) = 0$. The heat flow in the vicinity of the ridge crest is raised in accordance with the reduction of u.

The effect of reducing the value of the partial melt in the numerical example is to lengthen the intrusion zone and increase the thickness of the plate close to the ridge crest. The temperature distribution on the vertical walls, as well as the relationship between u and the melt fraction are shown in Fig. 16. The shape of the underside of the lithosphere is well approximated by using Fig. 2 with the value of u appropriate to the amount of partial melt.

Conclusions

In an effort to match the ridge elevation, we were able to find a value of $\Delta\rho$ such that the predicted and observed elevations were in agreement everywhere except near the ridge crest. Davis & Lister (1974) have plotted ridge elevation as a function of

$\sqrt{t}$ and shown that for profiles longer than 10 My the height of the ridge crest consistently lies 200–300 m below the $x = 0$ intercept of a straight line fitting the observations. The existence of an intrusion zone in the physical model reduces this discrepancy but cannot be the sole cause of it. For the Pacific, with a spreading rate of 40 mm/year, the thickness of the intrusion zone was 0·8 km, and this reduced the deviation by only 30 m. The thickness of the intrusion zone increases with decreasing spreading rates but the standard deviations of ridge crest elevations are too large to detect any dependence of this deviation on spreading velocity.

An arbitrary amount of hydrothermally cooled lithosphere can be added on top of that generated by the physical model without violating the heat flow equations. The depression at the ridge crest can be accounted for if a few kilometre thick layer of water-cooled material exists and if conduction gradually replaces convection as the dominant heat transport mechanism so that this layer vanishes by a crustal age of 4 or 5 My. This amounts to an artificial lengthening of the intrusion zone in equation (19) and is the essence of a suggestion put forth by Davis & Lister (1974) to explain the depression. Alternatively, this phenomenon might be the response of a floating solid plate to the dynamics of flow of a viscous fluid beneath. Whatever the cause, the misfit between predicted and observed elevations at the ridge crest are significant and additional modifications to the model are required to explain this deviation.

It is also possible to speculate that there is an additional mechanism which should raise the predicted elevation of the ridge crest, assuming that region is in isostatic equilibrium. If an appreciable volume of partial melt exists below the ridge, an associated 10 per cent density change from liquid to solid would require that this material have a density considerably less than the rest of the asthenosphere, and this buoyant mass should increase the height of the predicted elevation and make the misfit between observation and prediction even worse. For example, a 6 km thick section of 25 per cent partial melt would raise the ridge crest by about 200 m.

The heat flow predicted by the model is in moderately good agreement with observations (see Figs 4(b) and 13). Nevertheless, Sclater & Francheteau (1970) have specified the mean heat flow at 15 My to be $0{\cdot}0922 \pm 0{\cdot}00447$ W m^{-2} and this value lies below the predicted values from any of the models. If the heat flow from the physical model is to be adjusted to fall within these bounds, then changes to the values of the material parameters are required. Equation (20) shows that a lowering of the heat flow is most easily effected by reducing the value of the melting temperature, but changes in the values of k or c_p may prove important.

The free-air gravity anomaly predicted by the physical model is positive over the ridge crest and the magnitude increases with decreasing spreading rates. Variations in the values of partial melt and allowing temperature gradients in the asthenosphere will not drastically alter the predicted free-air gravity anomaly if the value of $\Delta\rho$ is adjusted to make the predicted and observed elevations agree.

Unfortunately, the rough topography over slow spreading ridges makes it difficult to determine what the maximum value of the gravity anomaly would have been had the surface of the lithosphere been smooth. Fast spreading ridges on the other hand, are often associated with rather smooth topography, and the flatness of the free-air gravity anomaly may provide a constraint on the cause of the depression of the ridge elevation. If the ridge is in isostatic equilibrium and the depression is caused by adding a layer of hydrothermally cooled rock, the free-air gravity anomaly will be only slightly decreased over that predicted from the model. If the depression is the result of viscous flow, then an absence of mass beneath the ridge crest may significantly reduce the anomaly. The flatness of the observed gravity anomaly over the East Pacific Rise and the 10 mgal misfit there may already be the result of viscous flow beneath the ridge.

We have shown that the rate of growth of the lithosphere is determined by a heat

budget and that important sources of heat may be latent heat of fusion and that associated with temperature gradients in the asthenosphere when these gradients exceed the melting point gradient. The existence of a free parameter, $\Delta\rho$, permits a wide range of contributions from either of these heat sources such that the resultant lithospheres still satisfy geophysical observations. When the only heat source is latent heat, the partial melt must exceed 30 per cent or thicknesses greater than 130 km will occur at a crustal age of 100 My. Also, such a large melt fraction, if it exists, must be confined to a narrow zone beneath the solid plate. When heat from temperature gradients in the asthenosphere are admitted into the model, the rate of thickening of the plate can remain small even when the percentage of partial melt is reduced to a very small value, ~ 1 per cent. Lithospheres grown under such conditions indicate a greater amount of misfit between the predicted and observed elevations of the ridge crest (see Fig. 13), but otherwise provide an acceptable fit to the observed heat flow and elevation.

Near the ridge crest, latent heat is probably the major source of heat and full solutions to the heat flow equation with boundary conditions have been obtained for various amounts of partial melt and different relationships between $\overline{T}(z)$, and time averaged temperature on the intrusion zone, and $T_f(z)$, the final temperature to which the magma cools before the next intrusion episode. A decrease in the value of partial melt increases the dimensionless velocity u, and hence lengthens the intrusion zone. Conversely, if $\overline{T}(z) > T_f(z)$, the intrusion zone is shortened.

The result of this study indicates that the physical model described by Parker & Oldenburg (1973), with some minor modifications, predicts a growth of the lithosphere, ridge elevation, heat flow, and free-air gravity anomaly in good agreement with geophysical observations. Only the elevation in the vicinity of the ridge crest cannot be predicted by this physical model and the discrepancy there may be in response to viscous flow beneath the floating plate or an artificial lengthening of the intrusion zone resulting from hydrothermal circulation.

University of California,
San Diego,
Institute of Geophysics and Planetary Physics,
La Jolla, California 92037.

References

Anderson, D. L. & Sammis, C., 1970. Partial melting in the upper mantle, *Phys. Earth Planet. Int.*, **3**, 41–50.

Anderson, D. L., Sammis, C. & Jordan, T., 1971. Composition and evolution of the mantle and core, *Science*, **171**, 1103–1112.

Bass, M. N., 1971. Variable alupsal basalt populations and their relation to sea floor spreading rates, *Earth Planet. Sci. Letts*, **11**, 18–22.

Bateman Manuscript Project, 1954. Ed. A. Erdèlyi, McGraw–Hill Book Co., Inc., New York.

Carslaw, H. S. & Jaeger, J. C., 1959 (Second Edition) *Conduction of heat in solids*, 58, Clarendon Press, London.

Clark, S. P., (Editor), 1966. *Handbook of physical constants* (Revised Edition), Geological Society of America, Inc., Memoir 97.

Davis, E. E. & Lister, C. R. B., 1974. Fundamentals of Ridge Crest Topography, *Earth Planet. Sci. Letts*, **21**, 405–413.

Deffeyes, K. S., 1972. Plume convection with an upper-mantle temperature inversion, *Nature*, **240**, 539–544.

Dziewonski, A. M., 1971. Upper mantle models from 'pure-path' dispersion data, *J. geophys. Res.*, **76**, 2587–2601.
Forsythe, D. W., 1974. *Anisotropy and the structural evolution of the oceanic upper mantle*, PhD Thesis, Massachusetts Institute of Technology.
Ito, K. & Kennedy, G. C., 1967. Melting and phase relations in a natural peridotite to 40 km., *Am. J. Sci.*, **265**, 519–538.
Kahle, H. G. & Talwani, M., 1973. Gravimetric Indian Ocean Geoid, *Z. Geophys.*, **39**, 167–187.
Kay, R., Hubbard, N. J. & Gast, P. W. 1970. Chemical characteristics and origin of oceanic ridge volcanic rocks, *J. geophys. Res.*, **75**, 1585–1613.
Leeds, A. R., 1974. *Rayleigh wave dispersion in the Pacific Basin*, PhD Thesis, University of California, Los Angeles.
LePichon, X. & Langseth, M. G., 1969. Heat flow from the MidOcean Ridges and sea-floor spreading, *Tectonophysics*, **8**, 319–344.
Lister, C. R. B., 1972. On the thermal balance of a Mid-Ocean Ridge, *Geophys. J. R. astr. Soc.*, **26**, 515–535.
McKenzie, D. P., 1967. Some remarks on heat flow and gravity anomalies, *J. geophys. Res.*, **72**, 6261–6273.
Molnar, P. & Oliver, J., 1969. Lateral variations of attenuation in the upper mantle and discontinuities in the lithosphere, *J. geophys. Res.*, **74**, 2648–2682.
Oldenburg, D. W. & Brune, J. N., 1972. Ridge transform fault spreading pattern in freezing wax, *Science*, **178**, 301–304.
Oldenburg, D. W. & Brune, J. N., 1974. An Explanation for the Orthogonality of Ocean Ridges and Transform Faults, *J. geophys. Res.*, **80**, 2575–2585.
Parker, R. L., 1973. The rapid calculation of potential anomalies, *Geophys. J. R. astr. Soc.*, **31**, 447–455.
Parker, R. L. & Oldenburg, D. W., 1973. Thermal model of ocean ridges, *Nature Phys. Sci.*, **242**, 137–139.
Pitman, W. C. & Talwani, M., 1972. Sea-floor spreading in the North Atlantic, *Bull. Geol. Soc. Am.*, **83**, 619–646.
Sclater, J. G. & Francheteau, J., 1970. The implications of terrestrial heat flow observations on current tectonic and geochemical models of the crust and upper mantle of the Earth, *Geophys. J. R. astr. Soc.*, **20**, 509–542.
Sclater, J. G., Anderson, R. N. & Bell, M. L., 1971. Elevation of ridges and evolution of the central Eastern Pacific, *J. geophys. Res.*, **76**, 7888–7915.
Solomon, S. C., 1973. Shear wave attenuation and melting beneath the Mid-Atlantic Ridge, *J. geophys. Res.*, **78**, 6044–6059.
Talwani, M., LePichon, X. & Ewing, M., 1965. Crustal structure of Mid-Ocean Ridges, *J. geophys. Res.*, **70**, 341–352.
Wyllie, P. J., 1971. *The dynamic Earth*, John Wiley & Sons, Inc., New York.

Appendix A

Green's function for a quarter space

The Eulerian steady-state heat flow equation is

$$\nabla^2 T - 2u\frac{\partial T}{\partial x} = 0 \tag{1}$$

where $T(x, z)$ is defined for $x \geqslant 0$, $z \leqslant 0$ and u is the dimensionless velocity. Define

$$T_1(x, z) = \begin{cases} T(x, z) & z \geqslant 0 \\ -T(x, z) & z \leqslant 0 \end{cases}$$

and let

$$\mathscr{T}_1(x,k) = \int_{-\infty}^{\infty} T_1(x,z)\exp(-ikz)dz$$

be the Fourier transform of $T_1(x,z)$. If we replace T by T_1 in equation (1) and take the Fourier transform we obtain

$$\mathscr{T}_1(x,k) = \mathscr{T}_1(0,k)\exp\left(-(\sqrt{[u^2+k^2]}-u)x\right). \tag{2}$$

Take the inverse Fourier transform of equation (2) and interchange the order of integration. Then

$$T(x,z) = \frac{\exp(ux)}{2\pi}\int_{-\infty}^{\infty} T_1(0,z')dz' \int_{-\infty}^{\infty} \exp\left(ik(z-z')\right)\exp\left(-\sqrt{(u^2+k^2)}x\right)dk.$$

The second integral, with the factor $\exp(ux)/2\pi$ is by definition $G(x,z;z')$, the Green's function for the problem. Hence*

$$G(x,z;z') = \frac{ux}{\pi}\exp(ux)\frac{K_1\left(u\sqrt{[(z-z')^2+x^2]}\right)}{\sqrt{(z-z')^2+x^2}}.$$

If temperatures are prescribed on the vertical axis for only $z \geqslant 0$ then we obtain

$$T(x,z) = \frac{ux\exp(ux)}{\pi}\int_0^{\infty} T(0,z')\left\{\frac{K_1\left(u\sqrt{[(z-z')^2+x^2]}\right)}{\sqrt{[(z-z')^2+x^2]}} - \frac{K_1\left(u\sqrt{[(z+z')^2+x^2]}\right)}{\sqrt{[(z+z')^2+x^2]}}\right\}dz'.$$

Appendix B

A differential equation for the isofuse line

We define the isofuse line to be that on which the equation

$$\hat{n}.\vec{v}\rho L = -k\frac{\partial T}{\partial n} \tag{1}$$

is obeyed. Parametrize the curve by $x = x(s)$ and $z = z(s)$. Then $\hat{n} = -\hat{x}z' + \hat{z}x'$ where $z' = dz/ds$ and $x' = dx/ds$. If $\vec{v} = \hat{x}v$ then equation (1) becomes

$$(-\hat{x}z'+\hat{z}x').\hat{x}v\rho L = -k(-\hat{x}z'+\hat{z}x').\left(\hat{x}\frac{\partial T}{\partial x} + \hat{z}\frac{\partial T}{\partial z}\right)$$

or

$$\frac{dz}{ds} = \frac{dx}{ds}\left(\frac{\partial T/\partial z}{(\rho vL/k)+(\partial T/\partial x)}\right). \tag{2}$$

The slope at any point (x,z) on the isofuse line is therefore given by

$$\frac{dz}{dx} = \left(\frac{\partial T/\partial z}{(\rho vL/k)+(\partial T/\partial x)}\right).$$

If the isofuse line is denoted by $z = Z(x)$ we obtain the desired result

$$\frac{dZ(x)}{dx} = \left(\frac{\partial T/\partial z}{(\rho vL/k)+(\partial T/\partial x)}\right)_{z=Z(x)} \tag{3}$$

or if we scale temperatures by T_m, lengths by l, and let $H = L/c_p\,T_m$ and $u = \rho c_p\,vl/2k$ we obtain equation in dimensionless form

$$\frac{dZ(x)}{dx} = \left(\frac{\partial T/\partial z}{2uH+(\partial T/\partial x)}\right)_{z=Z(x)}. \tag{4}$$

* Bateman Manuscript Project, p. 16, No. 26.